

Effect of Cyclic Voltammetry Activation in Hydrochloric Acid on the Oxygen Reduction Performance of Screen-Printed Gold Electrodes

Turgut Sönmez 

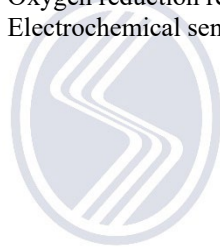
Karabük University, Faculty of Engineering and Natural Sciences, Department of Chemistry, Karabük, Türkiye, turgutsonmez@karabuk.edu.tr, ror.org/04wy7gp54

ARTICLE INFO

ABSTRACT

Keywords:

Screen-printed gold electrodes
Electrochemical surface activation
Cyclic voltammetry
Hydrochloric acid
Oxygen reduction reaction
Electrochemical sensing



Article History:

Received: 30.07.2025
Revised: 08.01.2026
Accepted: 09.01.2026
Online Available: 04.02.2026

Herein, screen-printed gold electrodes (SPGEs) were electrochemically activated via cyclic voltammetry in 0.5 M HCl, with the selection of HCl guided by preliminary comparisons of activation behaviour in different acidic media. Optimal surface activation was achieved after 12 cycles. Structural and morphological characterization by SEM-EDX and XRD revealed the development of a rougher, more porous surface and the formation of catalytically active gold oxide species. Electrochemical evaluation demonstrated a substantial enhancement in oxygen reduction reaction (ORR) performance, including a 120 mV positive shift in onset potential and a 27% increase in current density under similar experimental conditions compared to the unmodified electrode. The double-layer capacitance (C_{dl}) increased from 1.23 μF to 2.00 μF , indicating enhanced capacitive behaviour. Electrochemical impedance spectroscopy (EIS) further revealed a dramatic reduction in total charge transfer resistance (R_{ct}), decreasing from 79.14 Ω to 9.4 Ω , signifying improved interfacial electron transfer kinetics. These enhancements are attributed to a combination of factors, including removal of surface contaminants, chloride induced restructuring, increased conductivity, and greater exposure of catalytically active gold oxide sites. These performance improvements are particularly relevant for sensing applications, where SPGEs are widely used as practical and low-cost platforms for dissolved oxygen detection. This study highlights cyclic voltammetry in 0.5 M HCl as a simple and effective approach for improving the electrocatalytic performance of SPGEs in ORR and related sensing applications.

1. Introduction

Screen-printed electrodes (SPEs) are compact electrochemical devices that integrate the working, counter, and reference electrodes onto a single substrate, typically made of ceramic, polymer, plastic, alumina, or paper [1-4]. These integrated systems offer a practical and efficient alternative to the conventional three-electrode configuration, in which the electrodes are separate and immersed in a bulk solution (acidic, alkaline, or neutral) for electrochemical measurements [5].

Compared to traditional setups, SPEs offer numerous advantages for real-world

applications, including low cost, disposability, miniaturization (enabling low sample volume analysis), versatility, ease of fabrication, user-friendliness, and time efficiency [5, 6]. SPEs have been widely applied across various fields, with significant use in environmental monitoring. They have been employed to detect and quantify heavy metals (e.g., Cd(II), Pb(II), Hg(II), As(III), Cr(VI)), organic contaminants, pesticides, and radioelements such as uranium, as well as to monitor dissolved oxygen (O_2) levels for water quality assessment [7-12].

Beyond environmental applications, SPEs are also used in biomedical and clinical diagnostics

for the detection of bacteria, lactic acid in sweat or blood, glucose, DNA, and other biologically relevant analytes [6, 7, 13]. Their ability to provide rapid, sensitive, and selective measurements makes SPEs a popular alternative to conventional laboratory-based techniques, offering benefits such as reduced analysis time, minimal sample handling, and lower risk of contamination [2].

A wide range of SPEs have been developed using both carbon-based materials (such as carbon nanotubes [14], graphite [4], and graphene [15]) and metal-based materials, including gold [6, 16], silver [17, 18], palladium [19], and copper [20]. While carbon-based SPEs are more commonly used due to their low cost and broad availability, novel metal-based SPEs are increasingly being explored for applications requiring superior electrochemical performance [7]. Although their adoption is somewhat constrained by the higher cost of noble metals, metal-based SPEs (particularly gold screen-printed electrodes (SPGEs)) are frequently employed due to their excellent electrical conductivity, rapid electron transfer kinetics, chemical stability, wide potential window, and environmental compatibility [1, 5].

Surface activation of SPEs is a commonly applied pre-treatment step designed to remove surface contaminants and improve the electrode's electrochemical performance. This activation process enhances key surface properties such as electron transfer kinetics, conductivity, hydrophilicity, and surface roughness, which in turn contribute to increased sensitivity and selectivity in sensing applications [5, 21].

While various physical and chemical methods such as thermal activation, mechanical polishing, oxygen plasma treatment, and ultrasonic cleaning have been explored for this purpose [1, 5, 22-24], electrochemical pre-treatment remains the most widely adopted approach due to its simplicity, effectiveness, and minimal instrumentation requirements [5]. This often involves cyclic voltammetric scanning in acidic media to clean and activate the electrode surface, particularly in the case of metal-based SPEs such as gold [6]. Such procedures are known to significantly enhance electrochemical

responsiveness by increasing electroactive surface area, removing passivating layers or surface contaminants, improving conductivity, and promoting the availability of more active sites for interaction with target analytes [6]. These strategies are comprehensively discussed in a recent review by Crapnell et al. [5], which provides an in-depth overview of surface modification approaches and their implications for electroanalytical performance.

Several studies [6, 25, 26] have explored the electrochemical pre-treatment or activation of gold surfaces or electrodes using acidic media, particularly sulfuric acid (H_2SO_4), via cyclic voltammetry (CV). A recent study by Zakaria et al. [6] demonstrated that CV activation of SPGEs in 0.5 M H_2SO_4 significantly enhances oxygen reduction reaction (ORR) performance. Similarly, Garcia et al. [1] reported that electrochemical cleaning in 0.1 M perchloric acid (HClO_4) is a highly efficient method for improving the electrochemical activity of SPGEs. In another investigation, Stan et al. [3] evaluated various cleaning protocols and recommended a milder approach involving potential cycling in a mixed ferri/ferrocyanide solution (0.5 mM $\text{K}_4[\text{Fe}(\text{CN})_6]/\text{K}_3[\text{Fe}(\text{CN})_6]$) between -0.7 V and 0 V for just 2-3 cycles, identifying it as an optimal method for effective surface renewal with minimal degradation. These findings highlight the diversity of effective electrochemical activation strategies for SPGEs, depending on the application requirements and desired surface characteristics.

In the present study, commercially available screen-printed gold electrodes (SPGEs) from Metrohm were electrochemically activated in 0.5 M hydrochloric acid (HCl) via cyclic voltammetry. Prior to detailed investigations, activation behaviour in different acidic media (H_2SO_4 , HNO_3 and HCl) was compared, and preliminary voltammetric measurements showed that SPGEs exhibit markedly different responses in chloride media. Whereas H_2SO_4 produced the expected gold oxide formation and reduction peaks in the microampere current regime, HCl generated milliampere-scale currents and a single broad reduction feature, consistent with chloride-induced surface restructuring and Au-Cl complex formation [27].

These observations highlighted the distinct influence of chloride on SPGE surfaces and motivated the selection of HCl as the activation medium. The surface modification was then performed by applying up to 20 potential cycles at 100 mV s^{-1} ; the cathodic peak current increased until the 12th cycle and subsequently decreased, identifying the 12th cycle as the optimal activation point based on several repetitions using different SPGEs from the same batch. The modified and unmodified electrodes were structurally characterized using SEM-EDX and XRD.

Electrochemical measurements were carried out using cyclic voltametry, complemented by kinetic and electrochemical impedance spectroscopy analyses, while oxygen reduction reaction (ORR) performance of both modified and unmodified electrodes was compared to correlate activity enhancements induced by surface activation with structural features. The activated SPGEs exhibited improved ORR performance, including a more positive onset potential and higher current density. These improvements arise from a combination of factors, including removal of surface contaminants, chloride-driven restructuring, the presence of oxidized gold surface species, improved conductivity, and increased accessibility of electroactive sites associated with the roughened and more porous surface morphology. Overall, CV-based pre-treatment in dilute HCl provides a simple and effective approach to improve the electrochemical performance of SPGE.

2. Experimental

2.1. Materials

Hydrogen chloride (HCl, fuming 37%), Nitric acid (HNO₃, 70%), Sulphuric acid (H₂SO₄, 95–98%), potassium ferricyanide (K₃[Fe(CN)₆], Merck), potassium chloride (KCl, Riedel-de Haën). High-purity nitrogen (N₂) and oxygen (O₂) gas cylinders were purchased from Pelenkoğlu Company (Karabük, Türkiye). Deionized (DI) water, obtained from an MDS-8 series water purification system (Miprolab), was used for the preparation of all electrochemical solutions. All reagents were of analytical grade and used without any further purification.

2.2. Screen printed gold electrodes

Screen-printed gold electrodes (SPGEs) (Metrohm DropSens, 220AT) are commercially available and were purchased from Metrohm Türkiye. The electrodes are fabricated on a ceramic substrate with dimensions of $3.4 \times 1.0 \times 0.05 \text{ cm}$. Both the working and counter electrodes are made of gold (Au), while the reference electrode is composed of silver (Ag). The geometric surface area of the working electrode is 0.11 cm^2 , and the substrate thickness is 0.05 cm^2 .

2.3. Characterization

Scanning electron microscopy (SEM) images and energy-dispersive X-ray spectroscopy (EDX) mappings of unmodified and modified SPGEs were obtained using a Carl Zeiss Ultra Plus SEM system. The working electrodes were mounted on carbon tape and examined under an acceleration voltage of 10 kV. EDX analysis was conducted using a Bruker XFlash 6|10 detector integrated into the SEM system. All imaging and analysis were performed using SmartSEM software. A Rigaku Ultima IV diffractometer was used to perform X-ray diffraction (XRD) measurements for investigating the crystalline structure of the electrode materials. Measurements were performed with Cu K α radiation at a scanning rate of $1.2^\circ/\text{min}$, and data were collected over a 2θ range of 5° to 60° .

2.4. Electrochemical measurements-instrumentation, cell and electrolyte

All electrochemical measurements, including electrochemical impedance spectroscopy (EIS), were performed using a PalmSens4 potentiostat (PalmSens BV, Netherlands) equipped with the PSTrace 5.9 software package. A custom-designed 50 mL electrochemical cell with a fitted 3D-printed lid was used for all experiments, which were conducted at room temperature ($\sim 23^\circ \text{C}$). A three-electrode configuration was employed, consisting of a gold (Au) working electrode, a gold (Au) counter electrode, and a silver (Ag) reference electrode, all integrated into the screen-printed electrode. For surface modification experiments, freshly prepared 0.5 M H₂SO₄, HNO₃ and HCl were used as the electrolyte. CV and subsequent EIS

measurements were performed on both unmodified and modified SPGEs in a solution containing 10 mM potassium ferricyanide ($K_3[Fe(CN)_6]$) and 0.1 M potassium chloride (KCl). CV was conducted prior to EIS to determine the midpoint potentials between the oxidation and reduction peaks. These midpoint potentials (95 mV for unmodified and 105 mV for modified SPGEs) were then used as the DC bias during EIS measurements. In all cases, the modulation amplitude (AC potential) was set to 5 mV. CV measurements for determining the C_{dl} ,

and consequently ECSA were conducted at varying scan rates in 0.1 M KCl solution (neutral pH: ~ 7) at room temperature. Additionally, CV measurements to evaluate the ORR activity of unmodified and modified SPGEs were performed in the same electrolyte. For these experiments, the electrolyte (0.1 M KCl) was purged with high-purity nitrogen and subsequently with oxygen for at least 30 minutes prior to the measurements to ensure gas saturation. Origin software was used for all data analysis.

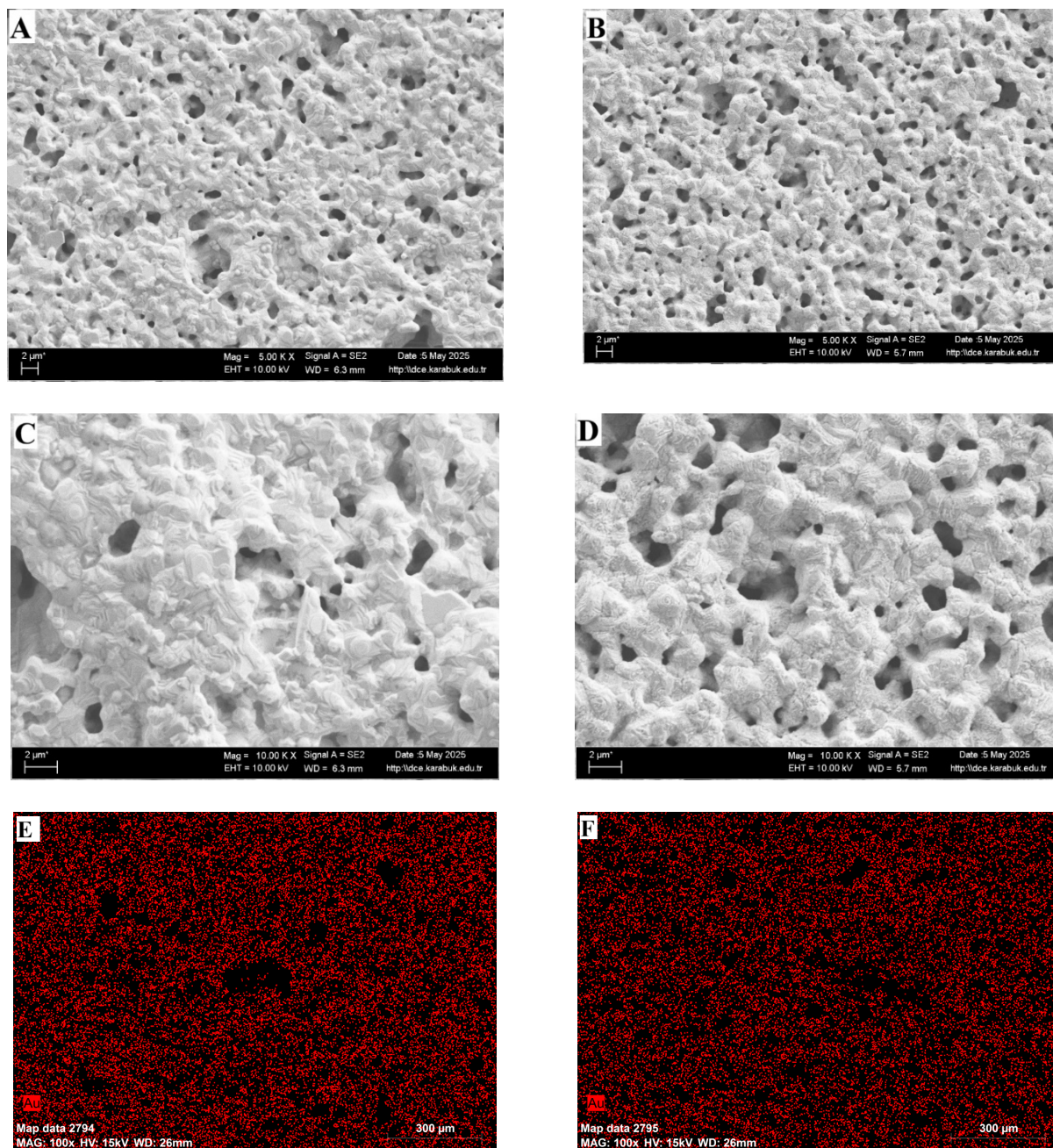


Figure 1. SEM images of (A) unmodified and (B) modified SPGEs at 5,000 \times magnification, and (C) unmodified and (D) modified SPGEs at 10,000 \times magnification. Scale bar: 2 μm . (E) Elemental mapping of gold on the unmodified electrode at 2,000 \times magnification (corresponding to the SEM image shown in Figure 3A), and (F) elemental mapping of gold on the modified electrode at 2,000 \times magnification (corresponding to the SEM image in Figure 3B)

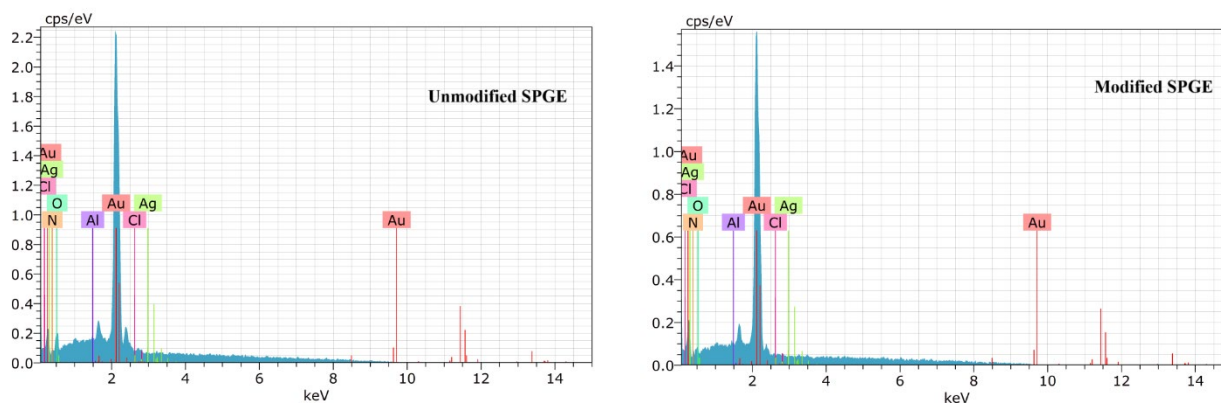


Figure 2. EDX analysis of unmodified (**left**) and modified (**right**) SPGEs at 100 \times magnification, focused on the electrode surface

3. Results and Discussion

3.1. Structural characterization

Since the electrode surface was modified in an acidic environment (0.5 M HCl) via electrochemical treatment, SEM was employed to investigate changes in surface morphology. Figures 1a-d display SEM images of both unmodified and modified SPGEs at two magnifications: 5,000 \times and 10,000 \times . At 5,000 \times magnification, the unmodified electrode (Figure 1a) exhibits a relatively smooth and uniform surface. In contrast, the modified electrode (Figure 1b) shows a significantly rougher texture, characterized by pronounced surface irregularities and the presence of pores (indicative of successful surface modification). At 10,000 \times magnification, the modified electrode (Figure 1d) appears substantially more porous and textured compared to the smoother morphology of the unmodified electrode (Figure 1c).

Elemental mapping of gold (Au) content, shown in Figures 1e and 1f for the unmodified and modified electrodes respectively, reveals no substantial difference in Au distribution between the two surfaces. This suggests that the modification process did not significantly alter the bulk Au content exposed at the surface at the magnification level used for mapping. These morphological changes clearly demonstrate that electrochemical activation under 0.5 M HCl conditions significantly alters the electrode surface by increasing roughness and porosity (properties commonly associated with enhanced electrochemical performance and a larger electroactive surface area). These observations will be further supported by electrochemical

characterization presented in the following sections.

As shown in Figure 2, EDX analysis revealed the presence of several elements on the electrode surfaces, including Au, Ag, Cl, O, N, and Al. As expected, Au exhibited the most intense peak in both unmodified and modified SPGEs, confirming the dominant presence of gold at the working electrode. However, a clear reduction in the gold peak intensity was observed following surface activation: the Au peak intensity decreased from approximately 2.2 cps/eV in the unmodified SPGE to less than 1.5 cps/eV in the modified electrode. The peak intensities observed around 1.7 keV and 2.4 keV (appearing just before and after the main Au peak) also decreased on the surface of the modified SPGE, as shown in Figure 2. In EDX analysis, the intensity of an elemental peak correlates with how exposed or accessible that element is on the surface. Therefore, the reduced Au signal strongly suggests the formation of a surface layer (likely composed of gold oxides or other electrochemically formed species) that covers or blocks the underlying gold.

Complementary SEM images acquired at 2000 \times magnification (Figure 3A-B) were analysed to further examine the surface composition. The corresponding EDX data showed that the normalized weight percentage of Au increased from 89.06% in the unmodified SPGE to 91.88% in the modified SPGE (Tables 1-2). This apparent increase does not indicate a higher absolute gold content but instead reflects a shift in elemental ratios. It is likely caused by the presence of light elements (such as C, H, and O) in the modification layer, which are either undetected or poorly detected by EDX.

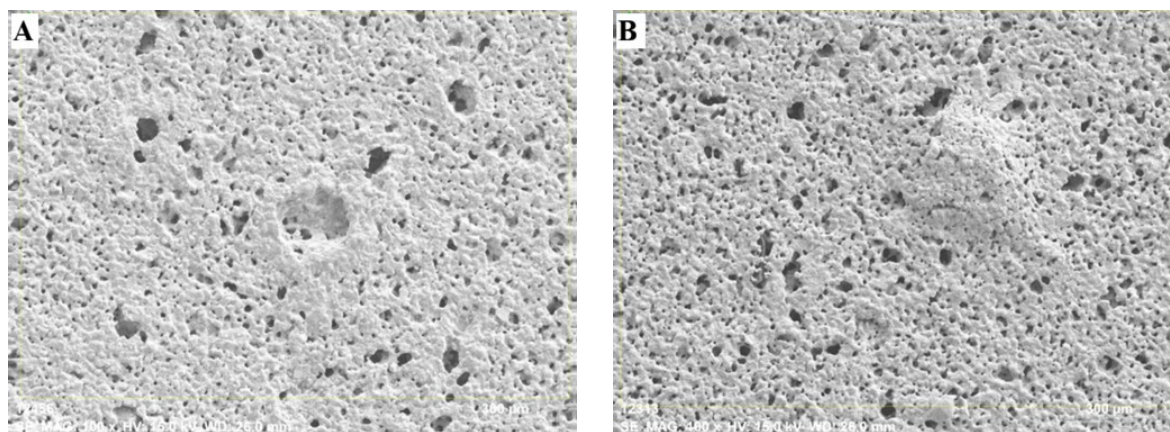


Figure 3. SEM images of (A) unmodified SPGE and (B) modified SPGE surfaces at 2000 \times magnification. These images correspond to the reference areas used for the EDX elemental analyses (Tables 1 and 2)

Table 1. EDX elemental composition of the unmodified SPGE surface corresponding to the SEM image shown in Figure 3A (2000 \times magnification)

Element	Atomic Number	Line Series	Weight % (unnormalized)	Weight % (normalized)	Atomic %	Error (wt.%)
N	7	K	2.91	3.34	21.84	± 0.89
O	8	K	4.75	5.45	31.15	± 1.06
Al	13	K	0.99	1.14	3.85	± 0.10
Cl	17	K	0.45	0.52	1.34	± 0.06
Ag	47	L	0.43	0.49	0.42	± 0.07
Au	79	M	77.63	89.06	41.39	± 2.99
Total	—	—	87.16	100.00	100.00	—

Table 2. EDX elemental composition of the modified SPGE surface corresponding to the SEM image shown in Figure 3B (2000 \times magnification)

Element	Atomic Number	Line Series	Weight % (unnormalized)	Weight % (normalized)	Atomic %	Error (wt.%)
N	7	K	2.93	3.20	24.26	± 1.09
O	8	K	2.86	3.12	20.74	± 0.90
Al	13	K	0.93	1.01	3.99	± 0.11
Cl	17	K	0.32	0.35	1.05	± 0.07
Ag	47	L	0.39	0.43	0.42	± 0.08
Au	79	M	84.23	91.88	49.54	± 3.29
Total	—	—	91.67	100.00	100.00	—

Their underrepresentation in the analysis artificially raises the relative percentage of heavier elements like Au. Together, the decrease in Au peak intensity and the increase in

normalized weight percentage support the conclusion that electrochemical modification in 0.5 M HCl leads to surface oxidation and the formation of a thin layer (such as Au₂O or

Au₂O₃) that alters the elemental accessibility and surface composition of the SPGE.

Figure 4 displays the XRD patterns of unmodified and modified SPGEs, alongside reference patterns for metallic gold (Au; COD ID: 9008463), gold (III) oxide (Au₂O₃; COD ID: 2105390), and the ceramic substrate used in SPGE fabrication. Due to the lack of available crystallographic data for metastable gold(I) oxide (Au₂O), no attempt was made to match potential corresponding peaks. Both unmodified and modified SPGEs exhibit clear reflections at approximately $2\theta \approx 38^\circ$ and 44° , corresponding to the (111) and (200) crystallographic planes of metallic Au, respectively [13]. Additional reflections observed at $\sim 26^\circ$, 28° , 35° , 43° , 54° , and 58° show good correspondence with the reference pattern for Au₂O₃, suggesting the presence of oxide-like phases on the electrode surfaces. Among these, the peaks near 35° and 54° are particularly pronounced and consistent with previously reported Au₂O₃ reflections, which may indicate preferred orientation of oxidized gold crystallites [28]. Notably, the modified SPGE exhibits an increase of $\sim 10\%$ in the relative intensities of the peaks at 26° , 28° , and 35° compared to the unmodified SPGE, consistent with an increased surface contribution from oxidized gold species, following electrochemical activation. However, because XRD is not inherently surface-sensitive and thin oxide layers may be below the detection depth, these features should be regarded as supportive but not definitive. Unambiguous determination of gold oxidation states (such as Au⁰, Au₂O, Au₂O₃) requires surface-sensitive techniques such as XPS, which will be considered in future work to complement the present analysis.

Importantly, distinct peaks arising from the ceramic substrate are also evident, particularly at $\sim 9^\circ$ and an intense broad peak centred around 27° , which are absent in the Au and Au₂O₃ reference patterns. These features can be attributed to the polycrystalline nature and composition of the underlying ceramic material, which contributes to the overall diffraction profile of both SPGE samples. These ceramic-related peaks do not overlap significantly with the characteristic Au or Au₂O₃ reflections and

thus do not interfere with the identification of surface gold phases.

While XRD has limited sensitivity for detecting amorphous or very low-concentration surface oxides, the enhanced intensity of oxide-related peaks in the modified SPGE, combined with consistent background contributions from the ceramic substrate, supports the successful modification of the electrode surface. Additional minor peaks are consistent with other components in the electrode structure, corroborated by elemental data from EDX shown in Figure 2.

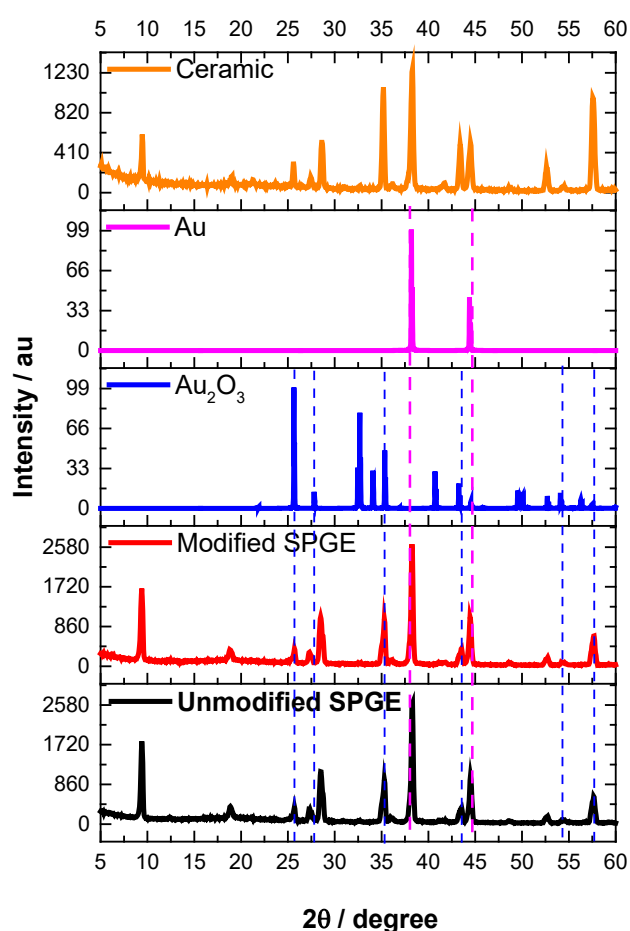


Figure 4. X-ray diffraction patterns of unmodified and modified SPGEs, along with reference patterns for gold oxide (Au₂O₃) and metallic gold (Au). Reflections from the ceramic substrate are also included for comparison. The measurements were performed at a scan rate of $1.2^\circ/\text{min}$ over a 2θ range of 5° to 60°

3.2. Electrochemical Studies

-Comparative Electrochemical Behaviour of SPGEs in Different Acidic Media

All electrochemical studies were conducted in a custom-designed electrochemical cell with an approximate volume of 50 mL, sealed using a 3D-printed lid to maintain stability and minimize contamination. First electrochemical study part was devoted to evaluating how different acidic environments effects the electrochemical behaviour of SPGEs, therefore cyclic voltammetry measurements were performed in 0.5 M H₂SO₄, HNO₃, and HCl under identical conditions. The resulting voltammograms in Figure 5a-c show that each acid produces a distinct electrochemical signature, reflecting different surface interactions and gold redox behaviours.

In H₂SO₄, the classical features of gold were observed, including well-defined gold oxide formation in the anodic sweep (around 0.8 V *vs.* Ag) and a prominent oxide reduction peak (around 0.6 V *vs.* Ag) during the cathodic sweep. These responses, recorded in the microampere range, are consistent with established behaviour of gold in sulfuric acid [6]. In contrast, CV recorded in HNO₃ showed two characteristic peaks around 0.0 and 0.1 V *vs.* Ag, which are typically associated with nitrate adsorption and surface-specific reduction processes [29]. The absence of a pronounced gold oxide reduction peak and the retention of microampere-scale currents indicate that nitrate induces only limited surface restructuring.

The most striking differences were observed in HCl, where the SPGE exhibited milliamper-

scale currents, three orders of magnitude higher than in H₂SO₄ and HNO₃. Additionally, the classical gold oxide formation region was largely suppressed, and only a single broad reduction peak appeared near ~ 0.5 V *vs.* Ag. This behaviour is consistent with strong chloride adsorption, formation of Au-Cl surface complexes, and chloride-driven surface reconstruction [27]. These mechanisms are known to increase surface roughness, expose new catalytic sites, and profoundly alter the double-layer structure. Collectively, these results demonstrate that HCl does not act as a simple substitute for H₂SO₄ but instead induces a fundamentally different surface chemistry on SPGEs. This provides a strong rationale for selecting HCl as the activation medium in this study, motivating a more detailed examination of its effects on surface modification and ORR performance.

-Electrochemical Activation of SPGEs in HCl for Enhanced ORR Performance

The surface modification experiments were performed using cyclic voltammetry in 0.5 M HCl at room temperature (~ 23 °C). As shown in Figure 6a, a nearly linear increase in cathodic peak currents was observed between the 1st and 12th cycles, indicating progressive electrochemical activation. This enhancement is attributed to both the removal of surface impurities and the generation of new electrochemically active sites through partial surface oxidation. Notably, a distinct cathodic peak appears around 0.5 V (*vs.* Ag), corresponding to the electrochemical reduction of hydrated gold oxide species formed during the anodic sweep.

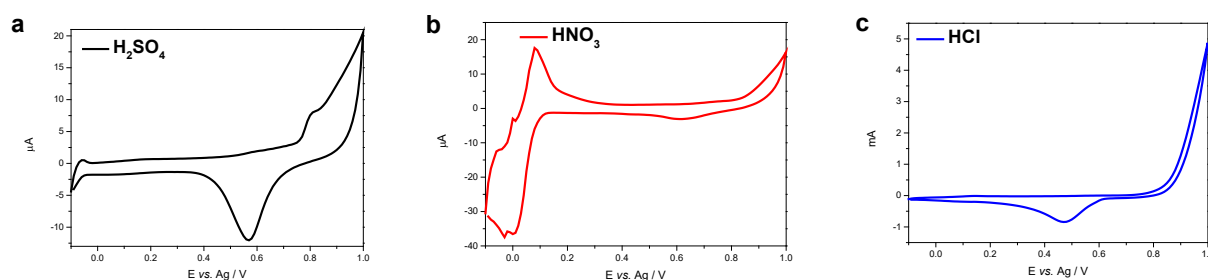


Figure 5. Cyclic voltammograms of SPGEs recorded in 0.5 M of a) H₂SO₄, b) HNO₃ and c) HCl. 100 mV s⁻¹ scan rate

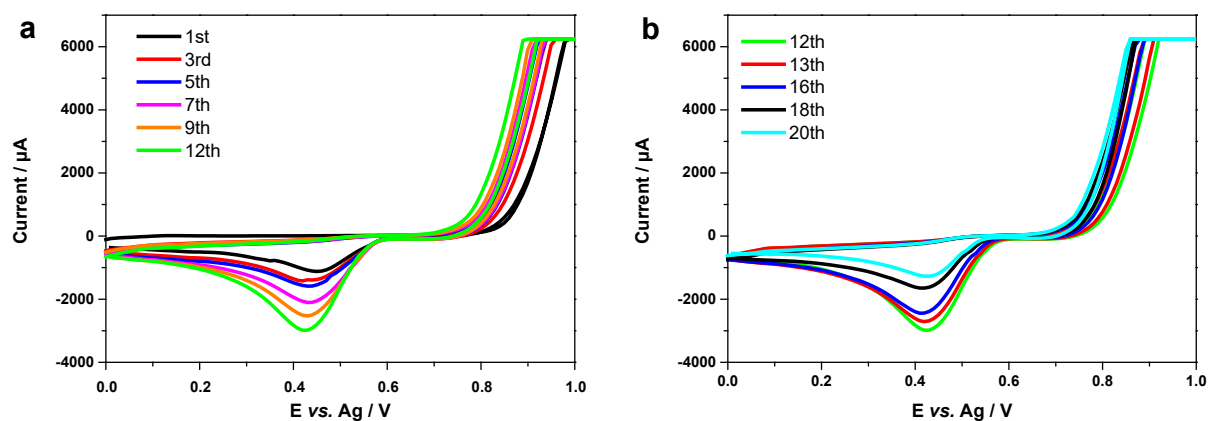
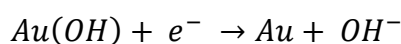


Figure 6. Cyclic voltammograms of the SPGE recorded in 0.5 M HCl at 100 mV s^{-1} scan rate. (a) Scans from the 1st to the 12th cycle, showing progressive surface activation. (b) Scans from the 12th to the 20th cycle, illustrating a decline in electrochemical performance due to over-cycling

This process aligns with the one-electron reduction of surface-bound gold hydroxide according to the reaction below [6, 30]:



This reaction mechanism, consistent with the findings of Zakaria et al. [6], reflects the redox cycling of gold hydroxide species. The increasing cathodic peak intensity suggests repeated formation and reduction of these oxide layers, which effectively clean the surface and enhance electron transfer kinetics. However, as shown in Figure 6b, continued cycling beyond the 12th scan results in a noticeable decline in peak current intensities. This performance degradation is likely due to surface over-oxidation or structural deterioration, which may reduce the number of accessible active sites and impair conductivity. Based on repeated trials within the same batch, 12 CV cycles were identified as the optimal activation protocol, providing a balance between surface activation, stability, and reproducibility.

After the electrochemical activation of the SPGE, its catalytic performance toward the oxygen reduction reaction (ORR) was evaluated in 0.1 M KCl. Figure 7a displays the forward scan voltammograms of the modified SPGE in both N_2 - and O_2 -purged electrolytes, alongside the unmodified SPGE measured in O_2 -saturated conditions. All currents were normalized to current density based on 0.11 cm^2 geometric surface area, and measurements were performed at 150 mV s^{-1} scan rate at room temperature. As shown in the voltammograms, significant

differences in ORR activity are evident between the modified and unmodified electrodes. The modified SPGE in N_2 -purged electrolyte shows no cathodic response, as expected due to the absence of dissolved O_2 , confirming that the observed cathodic currents in the oxygenated media are solely attributed to the reduction of O_2 . In contrast, the modified SPGE in O_2 -purged KCl demonstrates substantially improved ORR performance compared to the unmodified SPGE. One key indicator of this enhancement is the positive shift in onset potential. Using a standard current density threshold of -0.1 mA cm^{-2} for onset potential determination [6, 31], the unmodified SPGE exhibits an onset at -280 mV , while the modified SPGE shows an earlier onset at -160 mV , representing a positive shift of approximately 120 mV . This shift reflects a lower overpotential requirement for ORR at the modified electrode, indicating more favourable reaction kinetics and higher catalytic activity.

Furthermore, the limiting current density (a critical parameter reflecting mass transport efficiency and contributing to overall catalytic performance) is also enhanced after modification. At a representative potential of -0.43 V , the modified SPGE exhibits approximately a 27% increase in current density compared to the unmodified electrode. This suggests that the activation procedure not only improves electron transfer kinetics but also enhances the accessibility of catalytically active surface sites by more effectively exposing them through surface restructuring.

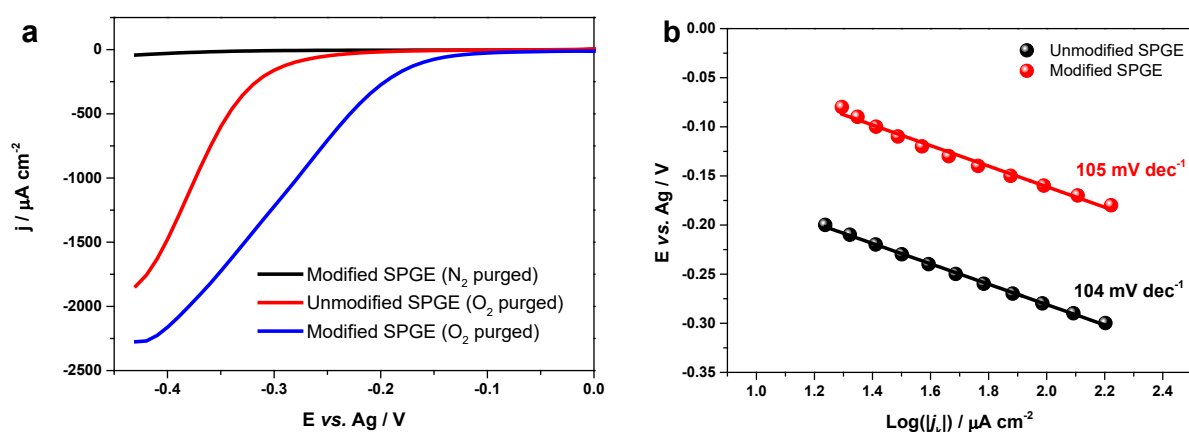


Figure 7. **a)** Cyclic voltammograms (forward scan only) of the modified SPGE in N₂-purged 0.1 M KCl (black), the unmodified SPGE in O₂-purged 0.1 M KCl (red), and the modified SPGE in O₂-purged 0.1 M KCl (blue) with 150 mV s⁻¹ scan rate. **b)** Corresponding Tafel plots with extracted Tafel slopes, derived from the linear region of the potential vs. Log (j_k) curves in the kinetic (low-current) region

These improvements can be attributed to the electrochemical cleaning and surface modification effects induced by cyclic voltammetry in 0.5 M HCl. The removal of organic or metallic contaminants, partial formation of surface gold oxide species, increased surface roughness, and the development of a more porous morphology collectively enhance the electrocatalytic performance. Additionally, the formation of hydrophilic oxide functionalities may facilitate better oxygen adsorption, further promoting enhanced ORR kinetics.

Tafel plots for both the modified and unmodified SPGEs are presented in Figure 7b. Analysis of the linear regions yielded Tafel slopes of 105 mV dec⁻¹ for the modified electrode and 104 mV dec⁻¹ for the unmodified one. Despite the significant improvements in onset potential and limiting current density observed for the modified SPGE, the near-identical Tafel slopes indicate that the fundamental ORR kinetics (particularly the rate-determining step and overall reaction mechanism) remain unchanged. While these values are slightly lower than the classical 120 mV dec⁻¹ typically associated with a rate-limiting first electron transfer to molecular oxygen [32], they are still broadly consistent with such a mechanism. Minor deviations from idealized Tafel slopes may arise from surface-specific effects, such as partial coverage by intermediates, double-layer charging, or mixed kinetic and mass transport control. Overall, the similarity in Tafel behaviour suggests that the observed activity enhancement arises primarily from surface activation and improved site

accessibility, rather than a change in the intrinsic ORR pathway.

To estimate the electrochemical double-layer capacitance (C_{dl}), which originates from the formation of an electrical double layer at the electrode-electrolyte interface, cyclic voltammetry was performed at varying scan rates in a non-Faradaic potential window [33]. The resulting C_{dl} values serve as a proxy for determining the electrochemically active surface area (ECSA), enabling the assessment of surface changes following modification. CV measurements were conducted in the potential range of 0.1-0.5 V vs. Ag, where no Faradaic processes occur, using scan rates ranging from 30 to 250 mV s⁻¹. The corresponding CV responses for unmodified and modified SPGEs are shown in Figures 8a and 8b, respectively. As expected, capacitive currents increased linearly with increasing scan rate, indicating dominant double-layer charging behaviour. Figure 8c shows a direct comparison at 200 mV s⁻¹, where the modified electrode exhibits a noticeably higher capacitive current. To quantify C_{dl} , the difference between anodic and cathodic currents ($\Delta I = I_a - I_c$) was plotted against $2v$ (v : scan rate) at a fixed potential of 0.3 V (Figure 8d) [34]. The slope of the resulting linear fit corresponds to the C_{dl} , as defined by Equation 1 [33].

$$I_a - I_c = C_{dl} \cdot 2v \quad (1)$$

From these plots, C_{dl} values of 1.27 μF and 2.00 μF were obtained for the unmodified and modified SPGEs, respectively (see Table 3). To estimate the ECSA, Equation 2 was applied,

where C_s is the specific capacitance per unit area [33]:

$$ECSA = \frac{C_{dl}}{C_s} \quad (2)$$

The value of C_s depends on several factors, including the electrode composition, surface structure, and the nature of the electrolyte [33, 35]. Based on XRD analysis, the SPGE exhibits dominant reflections corresponding to the Au(111) and Au(200) planes, confirming a polycrystalline structure with low-index facets. Literature reports [35, 36] indicate that C_s values for well-defined gold surfaces in near-neutral media (e.g., 0.05 – 0.1 M KCl or phosphate buffers) typically range between 14 and 25 $\mu\text{F cm}^{-2}$. In this study, a fixed value of $C_s = 14 \mu\text{F cm}^{-2}$ was selected, consistent with reported values for Au(111) in perchlorate electrolytes [35]. Using this reference, the calculated ECSA values are 0.091 cm^2 for unmodified SPGE, and 0.143 cm^2 for the modified one (see Table 3).

These results indicate an approximate 57% increase in both C_{dl} and ECSA after surface activation. However, this estimated ECSA increase must be interpreted cautiously considering subsequent observations. In Figure 9a, CVs recorded in 10 mM $\text{K}_3[\text{Fe}(\text{CN})_6]$ containing 0.1 M KCl (using the $[\text{Fe}(\text{CN})_6]^{3-}/[\text{Fe}(\text{CN})_6]^{4-}$ redox couple as a kinetic probe) show that the modified electrode exhibits higher Faradaic peak currents and slightly more positive peak potentials. Notably, there is no apparent difference in capacitive currents between the unmodified and modified SPGEs. This suggests that the enhancement in electrochemical activity is not due to an increase in the electrochemically active surface area, as inferred from C_{dl} , but is likely dominated by intrinsic surface changes such as increased microscopic porosity or exposure of more catalytically active sites. As previously noted, the C_s value depends on several factors including surface structure.

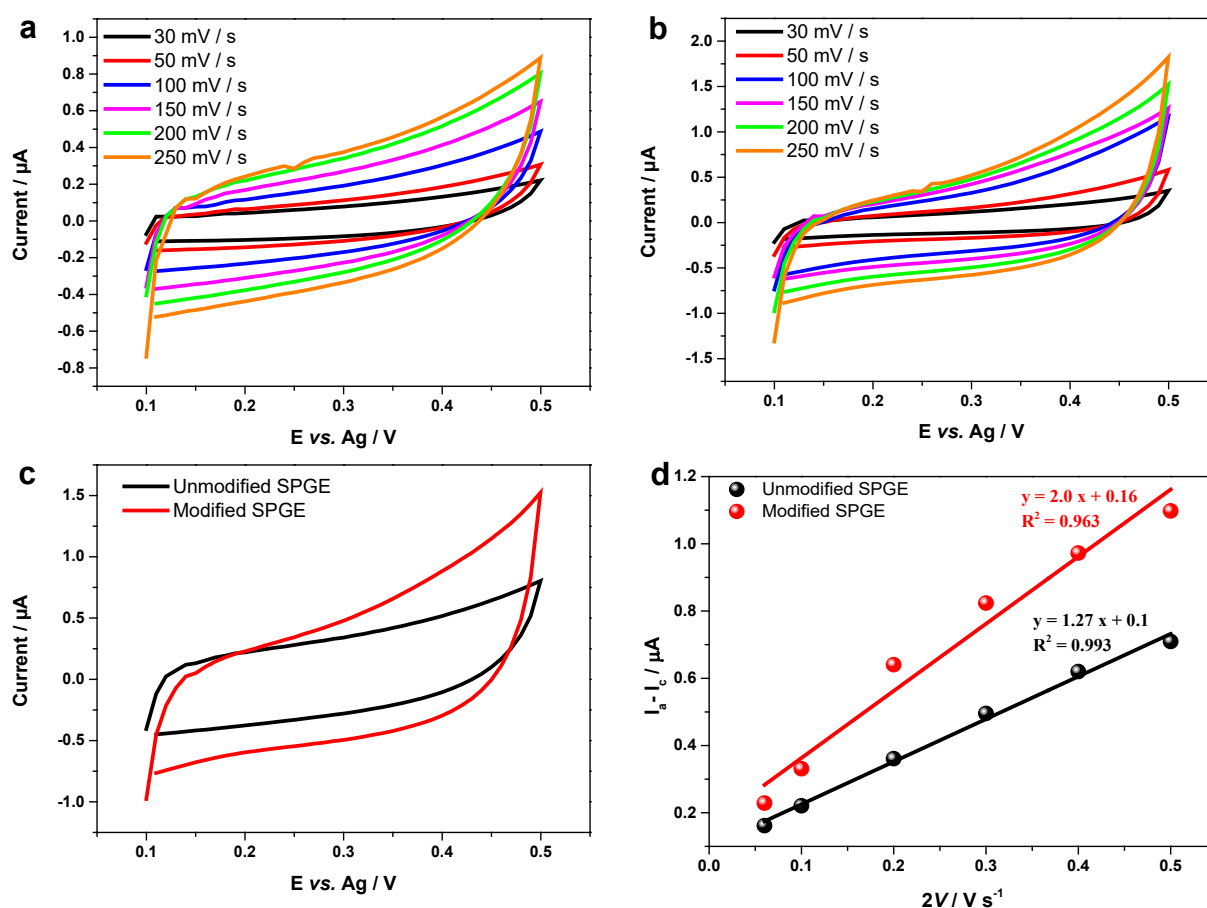


Figure 8. Cyclic voltammograms of (a) unmodified and (b) modified SPGEs recorded in 0.1 M KCl at scan rates varying from 30 mV s^{-1} to 250 mV s^{-1} within a non-Faradaic potential window (0.1 V - 0.5 V vs Ag).

(c) Comparison of CV responses for unmodified and modified SPGEs at 200 mV s^{-1} . (d) Plots of $\Delta I_a - I_c$ against $2v$ (v : 30, 50, 100, 150, 200, and 250 mV s^{-1}) at 0.3 V (vs. Ag), derived from the CV curves in a and b. The slope of each linear fit corresponds to the C_{dl} value, summarized in Table 3

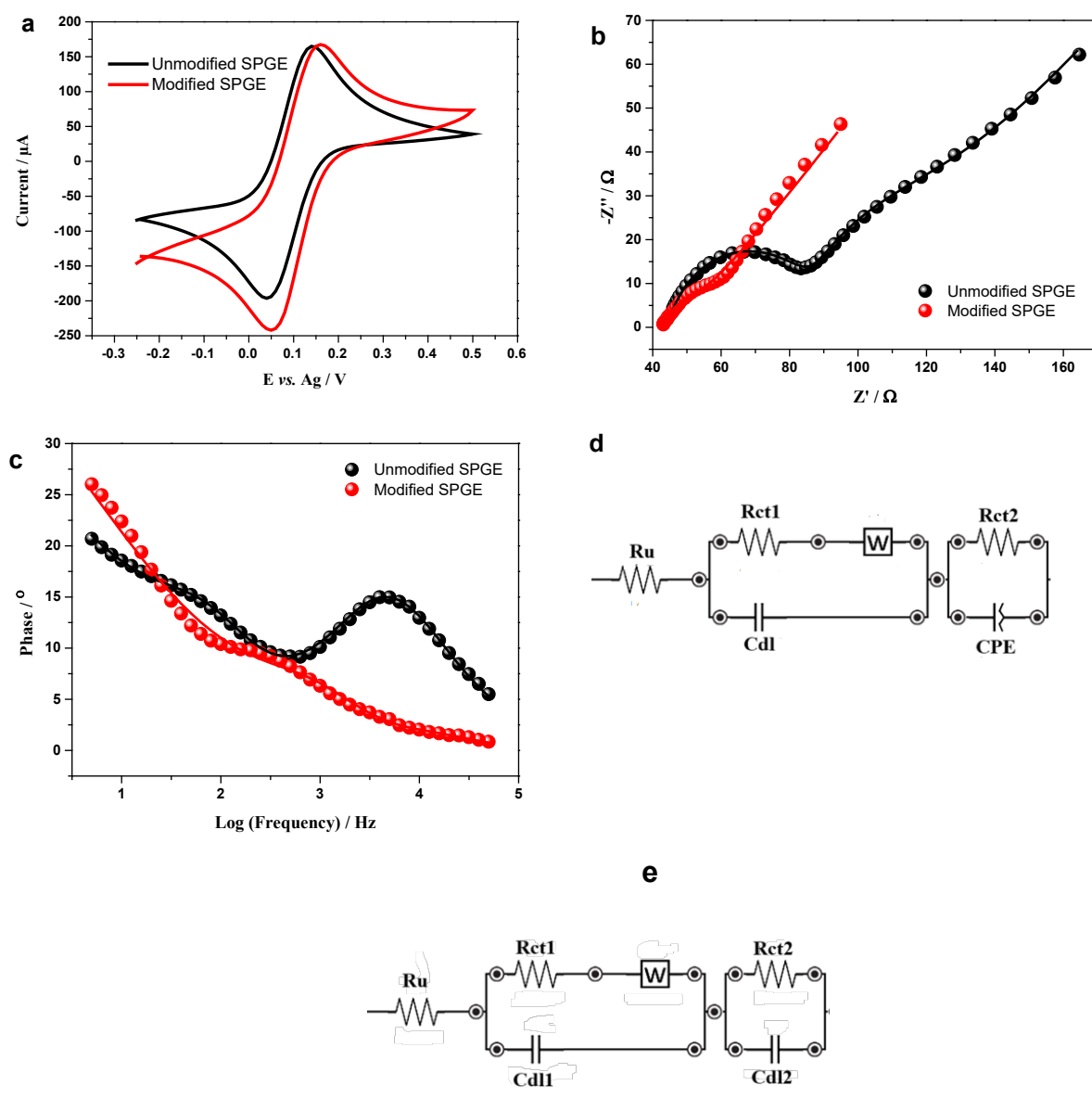


Figure 9. a) Cyclic voltammograms of unmodified and modified SPGE electrodes recorded in 10 mM $K_3[Fe(CN)_6]$ containing 0.1 M KCl at 100 mV s^{-1} . b) Nyquist Plots comparing the impedance responses of both electrodes. c) Bode plots of unmodified and modified SPGE electrodes. Modulation amplitude is 5 mV d) Equivalent circuit model used for fitting the unmodified-SPGE data. e) Equivalent circuit model used for fitting the modified-SPGE data. In the circuit diagrams: R_u represents the uncompensated solution resistance; C_{dl} is the double-layer capacitance; W denotes the Warburg impedance element; CPE is the constant phase element; R_{ct1} corresponds to the charge transfer resistance within the diffuse layer; and R_{ct2} represents the surface charge transfer resistance at the SPGE interface

Table 3. Summary of electrochemical parameters derived from CV and EIS measurements for unmodified and modified SPGEs

Electrode	$E_{-0.1 \text{ mA cm}^{-2}}$ (mV)	$j_{-0.43V}$ ($\mu\text{A cm}^{-2}$)	C_{dl} (μF)	ECSA (cm^2)	Total R_{ct} (Ω)
Unmodified SPGE	-280	1842	1.27 (± 0.05)	0.091	79.14 (± 1.16)
Modified SPGE	-160	2276	2.0 (± 0.17)	0.143	9.4 (± 0.47)

In this study, a fixed C_s was assumed for both electrodes to allow estimation of relative changes. However, surface restructuring (evident

from SEM images and supported by the observed increase in Faradaic response) suggests that the true enhancement arises from intrinsic porosity

and altered surface architecture, rather than an absolute increase in ECSA. Therefore, the improvement in electron transfer kinetics is better attributed to electrochemical activation in 0.5 M HCl, which effectively removes surface contaminants, restructures the electrode surface, and exposes reactive pore structures. These changes align with the improved ORR onset potential and current density, reinforcing the conclusion that surface activation enhances catalytic performance by modifying the physical microstructure rather than significantly enlarging the electroactive surface area.

To further assess the interfacial electron transfer characteristics of both unmodified and modified SPGEs, EIS measurements were carried out in a solution of 10 mM $K_3[Fe(CN)_6]$ containing 0.1 M KCl. Prior to impedance measurements, CVs were recorded (Figure 9a) to determine the mid-point potentials between the anodic and cathodic peaks. These potentials (0.095 V for the unmodified SPGE and 0.105 V for the modified SPGE) were subsequently used as the DC bias during EIS. Nyquist plots (Figure 9b) show a pronounced reduction in semicircle diameter for the modified SPGE, indicating a significant decrease in charge transfer resistance. Complementary Bode plots in Figure 9c further support this, with the modified electrode displaying a greater phase angle and lower overall impedance magnitude across a wide frequency range (both consistent with enhanced interfacial electron transfer).

The EIS data were quantitatively analysed using equivalent circuit modelling. For the unmodified SPGE, the circuit shown in Figure 9d was used. This model included uncompensated solution resistance (R_u), charge transfer resistance through the diffuse layer (R_{ct1}), and surface charge transfer resistance (R_{ct2}). When applied to the modified SPGE, however, this model resulted in relatively high fitting errors, particularly for R_{ct2} . To improve model accuracy, the constant phase element (CPE) was replaced with a double-layer capacitance (C_{dl2}) (Figure 9e), which significantly reduced the fitting error. The extracted fitting parameters for both electrodes are summarized in Table 4. After surface modification, both R_{ct1} and R_{ct2} decreased dramatically from 35.05 Ω to 7.97 Ω and from 44.09 Ω to 1.43 Ω , respectively, resulting in a

total R_{ct} reduction from 79.14 Ω to 9.4 Ω (Table 3). This substantial decrease reflects improved conductivity, and interfacial electron transfer efficiency, likely due to the formation of gold oxides, increased surface porosity, and exposure of more catalytically favourable sites [6].

Table 4. EIS-derived values of uncompensated resistance (R_u), diffuse layer charge transfer resistance (R_{ct1}), surface charge transfer resistance (R_{ct2}), fitting errors, and convergence fit values for unmodified and modified SPGEs, based on the equivalent circuits in Figures 9d and 9e using PCTrace 5.9 software

Electrode	Element	Value / Ω	Error / %
Unmodified SPGE	R_u	44.28	0.370
	R_{ct1}	35.05	2.031
	R_{ct2}	44.09	1.013
	Convergence fit value (X^2): 0.0000285		
Modified SPGE	R_u	42.88	0.803
	R_{ct1}	7.97	5.34
	R_{ct2}	1.43	28.34
	Convergence fit value (X^2):0.0002		

The improved fitting using C_{dl2} instead of CPE further supports the presence of structural and compositional changes after the activation surface in which the modified surface behaves more like a pure capacitor interface. Overall, the dramatic decrease in R_{ct} following electrochemical activation in 0.5 M HCl is strong evidence of enhanced electron transfer kinetics.

The impedance data confirm that the modification protocol significantly enhances the electrocatalytic properties of the SPGE by facilitating faster electron transfer, primarily due to increased conductivity and favourable surface restructuring. These results align well with earlier observations, such as the enhanced ORR onset potential and increased limiting current density and reinforce the conclusion that the benefits of acid activation stem from improved surface quality and accessibility of active sites, rather than from a mere increase in surface area.

4. Conclusion

Screen-printed gold electrodes were effectively activated via cyclic voltammetry in 0.5 M HCl,

with optimal surface modification achieved after 12 cycles. SEM-EDX and XRD analyses revealed that this treatment produced a rougher and more porous surface and promoted the formation of catalytically active gold oxide species, without altering the bulk composition of the electrode.

Electrochemical testing demonstrated substantial improvements in ORR activity, including a 120 mV positive shift in onset potential and a ~27% increase in current density relative to the unmodified electrode. Although C_{dl} and ECSA based estimates suggested an approximately 57% increase in electroactive surface area, ferricyanide redox measurements revealed no corresponding increase in double-layer charging current. This indicates that the observed enhancements primarily stem from intrinsic surface restructuring such as pore formation and exposure of more catalytically favourable regions rather than from a true enlargement of the geometric surface area. EIS measurements further supported this interpretation, revealing a significant reduction in charge transfer resistance (R_{ct}) at the electrode-electrolyte interface after activation, attributable to increased surface conductivity and more efficient interfacial electron transfer. The improved fitting obtained using a pure double-layer capacitance element further reinforces the presence of structural and compositional changes introduced by the activation process.

Overall, the enhanced electrocatalytic performance of the modified SPGE arises from a combination of factors, including contaminant removal, chloride-induced restructuring, increased conductivity, and improved accessibility of electroactive sites. These results demonstrate that CV activation in 0.5 M HCl represents a simple, and effective approach for tailoring SPGE surfaces to boost ORR activity and, by extension, improve their performance in oxygen-sensing and related electroanalytical applications. While the present study demonstrates clear improvements in electrocatalytic performance, it was conducted using SPGEs from a single commercial batch. Future studies involving multiple batches and suppliers will be valuable for further assessing reproducibility and general applicability.

Article Information Form

Funding

This work was supported by the Karabuk University Scientific Research Projects Coordination Unit under Project No. KBÜBAP-24-DS-143.

The Declaration of Conflict of Interest/ Common Interest

No conflict of interest or common interest has been declared by the author.

Artificial Intelligence Statement

Artificial intelligence tools were used solely for minor English grammatical and language corrections.

Copyright Statement

The author owns the copyright of their work published in the journal and their work is published under the CC BY-NC 4.0 license.

References

- [1] D. García García, et al., "Impact of cleaning procedures on screen-printed gold electrodes performance for mutation detection," *J. Appl. Electrochem.*, vol. 55, pp. 1937-1946, 2025. doi: 10.1007/s10800-025-02271-8. [Online]. Available: <https://doi.org/10.1007/s10800-025-02271-8>
- [2] R. D. Crapnell, A. G.-M. Ferrari, N. C. Dempsey, and C. E. Banks, "Electroanalytical overview: screen-printed electrochemical sensing platforms for the detection of vital cardiac, cancer and inflammatory biomarkers," *Sens. Diagn.*, vol. 1, no. 3, pp. 405-428, May 2022. doi: 10.1039/d1sd00041a. [Online]. Available: <https://pubs.rsc.org/en/content/articlehtml/2022/sd/d1sd00041a>
- [3] D. Stan, et al., "What is the optimal method for cleaning screen-printed electrodes?," *Processes*, vol. 10, no. 4, p. 723, Apr 2022. doi: 10.3390/pr10040723. [Online]. Available: <https://doi.org/10.3390/pr10040723>

- [4] J. Lee, G. Hussain, C. E. Banks, and D. S. Silvester, "Screen-printed graphite electrodes as low-cost devices for oxygen gas detection in room-temperature ionic liquids," *Sensors*, vol. 17, no. 12, p. 2734, Nov 2017. doi: 10.3390/s17122734. [Online]. Available: <https://doi.org/10.3390/s17122734>
- [5] R. D. Crapnell and C. E. Banks, "Electroanalytical overview: Screen-printed electrochemical sensing platforms," *ChemElectroChem*, vol. 11, p. e202400370, Oct 2024. doi: 10.1002/celec.202400370. [Online]. Available: <https://doi.org/10.1002/celec.202400370>
- [6] N. D. Zakaria, et al., "Electrochemical and imaging evaluations of electrochemically activated screen-printed gold electrodes," *Analyst*, vol. 149, no. 22, pp. 5401-5410, Nov 2024. doi: 10.1039/d4an00990h. [Online]. Available: <https://doi.org/10.1039/d4an00990h>
- [7] M. Li, Y.-T. Li, D.-W. Li, and Y.-T. Long, "Recent developments and applications of screen-printed electrodes in environmental assays—A review," *Anal. Chim. Acta*, vol. 734, pp. 31-44, July 2012. doi: 10.1016/j.aca.2012.05.018. [Online]. Available: <https://doi.org/10.1016/j.aca.2012.05.018>
- [8] E. Bernalte, C. M. Sánchez, and E. P. Gil, "Determination of mercury in ambient water samples by anodic stripping voltammetry on screen-printed gold electrodes," *Anal. Chim. Acta*, vol. 689, no. 1, pp. 60-64, Mar 2011. doi: 10.1016/j.aca.2011.01.042. [Online]. Available: <https://doi.org/10.1016/j.aca.2011.01.042>
- [9] R.-J. Zheng, Y.-M. Fang, S.-F. Qin, J. Song, A.-H. Wu, and J.-J. Sun, "A dissolved oxygen sensor based on hot electron induced cathodic electrochemiluminescence at a disposable CdS modified screen-printed carbon electrode," *Sens. Actuators B Chem.*, vol. 157, no. 2, pp. 488-493, Oct 2011. doi: 10.1016/j.snb.2011.05.005. [Online]. Available: <https://doi.org/10.1016/j.snb.2011.05.005>
- [10] J. P. Metters, R. O. Kadara, and C. E. Banks, "Electroanalytical sensing of chromium (III) and (VI) utilising gold screen printed macro electrodes," *Analyst*, vol. 137, no. 4, pp. 896-902, Feb 2012. doi: 10.1039/c2an16054d. [Online]. Available: <https://doi.org/10.1039/C2AN16054D>
- [11] J. Tu, Y. Gan, T. Liang, H. Wan, and P. Wang, "A miniaturized electrochemical system for high sensitive determination of chromium (VI) by screen-printed carbon electrode with gold nanoparticles modification," *Sens. Actuators B Chem.*, vol. 272, pp. 582-588, Nov 2018. doi: 10.1016/j.snb.2018.06.006. [Online]. Available: <https://doi.org/10.1016/j.snb.2018.06.006>
- [12] V. T. Kostaki, A. B. Florou, and M. I. Prodromidis, "Electrochemically induced chemical sensor properties in graphite screen-printed electrodes: The case of a chemical sensor for uranium," *Electrochim. Acta*, vol. 56, no. 24, pp. 8857-8860, Oct 2011. doi: 10.1016/j.electacta.2011.07.092. [Online]. Available: <https://doi.org/10.1016/j.electacta.2011.07.092>
- [13] M. Krishna, P. Neena, A. Pradeep, P. Vasu Suneesh, and T. Satheesh Babu, "Gold microflower modified screen-printed carbon electrode for the electrochemical detection of lactic acid in blood and sweat," *ChemCatChem*, vol. 16, no. 22, p. e202400999, Nov 2024. doi: 10.1002/cctc.202400999. [Online]. Available: <https://doi.org/10.1002/cctc.202400999>
- [14] J. Wang and M. Musameh, "Carbon nanotube screen-printed electrochemical sensors," *Analyst*, vol. 129, no. 1, pp. 1-2, Jan 2004. doi: 10.1039/B313431H. [Online]. Available: <https://doi.org/10.1039/B313431H>

- [15] C. Karuwan, A. Wisitsoraat, P. Chaisuwan, D. Nacapricha, and A. Tuantranont, "Screen-printed graphene-based electrochemical sensors for a microfluidic device," *Anal. Methods*, vol. 9, no. 24, pp. 3689-3695, June 2017. doi: 10.1039/c7ay00379j. [Online]. Available: <https://doi.org/10.1039/C7AY00379J>
- [16] F. Rueda-Holgado, E. Bernalte, M. Palomo-Marín, L. Calvo-Blazquez, F. Cereceda-Balic, and E. Pinilla-Gil, "Miniaturized voltammetric stripping on screen printed gold electrodes for field determination of copper in atmospheric deposition," *Talanta*, vol. 101, pp. 435-439, Nov 2012. doi: 10.1016/j.talanta.2012.09.054. [Online]. Available: <https://doi.org/10.1016/j.talanta.2012.09.054>
- [17] J.-M. Zen, C.-C. Yang, and A. S. Kumar, "Voltammetric behavior and trace determination of Pb²⁺ at a mercury-free screen-printed silver electrode," *Anal. Chim. Acta*, vol. 464, no. 2, pp. 229-235, July 2002. doi: 10.1016/S0003-2670(02)00472-5. [Online]. Available: [https://doi.org/10.1016/S0003-2670\(02\)00472-5](https://doi.org/10.1016/S0003-2670(02)00472-5)
- [18] W. Tang, K. Fan, J. Zhou, J. Wu, and F. Ji, "Unmodified screen-printed silver electrode for facile detection of organophosphorus pesticide," *Ionics*, vol. 21, no. 2, pp. 587-592, Feb 2015. doi: 10.1007/s11581-014-1358-y. [Online]. Available: <https://link.springer.com/article/10.1007/s11581-014-1358-y>
- [19] J. P. Metters, F. Tan, and C. E. Banks, "Screen-printed palladium electroanalytical sensors," *J. Solid State Electrochem.*, vol. 17, no. 6, pp. 1553-1562, June 2013. doi: 10.1007/s10008-013-2041-3. [Online]. Available: <https://link.springer.com/article/10.1007/s10008-013-2041-3>
- [20] A. Nyabadza, A. Plouze, S. Heidarinasab, M. Vazquez, and D. Brabazon, "Screen-printed electrodes on paper using copper nano-and micro-particles," *J. Mater. Res. Technol.*, vol. 29, pp. 5189-5197, Mar 2024. doi: 10.1016/j.jmrt.2024.03.016. [Online]. Available: <https://doi.org/10.1016/j.jmrt.2024.03.016>
- [21] S. M. da Silva, et al., "Improved anodic stripping voltammetric detection of zinc on a disposable screen-printed gold electrode," *Ionics*, vol. 26, no. 5, pp. 2611-2621, May 2020. doi: 10.1007/s11581-019-03379-6. [Online]. Available: <https://doi.org/10.1007/s11581-019-03379-6>
- [22] R. Gusmão, et al., "Enhanced electrochemical sensing of polyphenols by an oxygen-mediated surface," *RSC Adv.*, vol. 5, no. 7, pp. 5024-5031, Jan 2015. doi: 10.1039/c4ra12660b. [Online]. Available: <https://doi.org/10.1039/C4RA12660B>
- [23] Y. L. Su, C. Y. Tai, and J. M. Zen, "A simple method to tune up screen-printed carbon electrodes applicable to the design of disposable electrochemical sensors," *Electroanalysis*, vol. 25, no. 11, pp. 2539-2546, Nov 2013. doi: 10.1002/elan.201300382. [Online]. Available: <https://doi.org/10.1002/elan.201300382>
- [24] S. Wang, K. Chang, and C.-J. Yuan, "Enhancement of electrochemical properties of screen-printed carbon electrodes by oxygen plasma treatment," *Electrochim. Acta*, vol. 54, no. 21, pp. 4937-4943, Aug 2009. doi: 10.1016/j.electacta.2009.04.006. [Online]. Available: <https://doi.org/10.1016/j.electacta.2009.04.006>
- [25] Y. Wang, et al., "Activation effect of electrochemical cycling on gold nanoparticles towards the hydrogen evolution reaction in sulfuric acid," *Electrochim. Acta*, vol. 209, pp. 440-447, Aug 2016. doi:

- 10.1016/j.electacta.2016.05.095. [Online]. Available: <https://doi.org/10.1016/j.electacta.2016.05.095>
- [26] W. Zhang, A. D. Bas, E. Ghali, and Y. Choi, "Passive behavior of gold in sulfuric acid medium," *Trans. Nonferrous Met. Soc. China*, vol. 25, no. 6, pp. 2037-2046, June 2015. doi: 10.1016/S1003-6326(15)63813-4. [Online]. Available: [https://doi.org/10.1016/S1003-6326\(15\)63813-4](https://doi.org/10.1016/S1003-6326(15)63813-4)
- [27] W. Gao, T. A. Baker, L. Zhou, D. S. Pinnaduwege, E. Kaxiras, and C. M. Friend, "Chlorine adsorption on Au (111): chlorine overlayer or surface chloride?," *J. Am. Chem. Soc.*, vol. 130, no. 11, pp. 3560-3565, Mar 2008. doi: 10.1021/ja077989a. [Online]. Available: <https://doi.org/10.1021/ja077989a>
- [28] N. Weiher, E. Willneff, C. Figulla-Kroschel, M. Jansen, and S. Schroeder, "Extended X-ray absorption fine-structure (EXAFS) of a complex oxide structure: a full multiple scattering analysis of the Au L3-edge EXAFS of Au₂O₃," *Solid State Commun.*, vol. 125, no. 6, pp. 317-322, Feb 2003. doi: 10.1016/S0038-1098(02)00817-7. [Online]. Available: [https://doi.org/10.1016/S0038-1098\(02\)00817-7](https://doi.org/10.1016/S0038-1098(02)00817-7)
- [29] T. Rabbow, N. Junker, C. Kretschmar, M. Schneider, and A. Michaelis, "Electrochemically induced degradation of screen-printed gold thick films," *J. Ceram. Sci. Technol.*, vol. 3, pp. 199-210, Dec 2012. doi: 10.4416/JCST2012-00023. [Online]. Available: https://www.ceramic-science.com/articles/all-articles.html?article_id=100202
- [30] N. D. Zakaria, et al., "Effect of supporting background electrolytes on the nanostructure morphologies and electrochemical behaviors of electrodeposited gold nanoparticles on glassy carbon electrode surfaces," *ACS Omega*, vol. 6, no. 38, pp. 24419-24431, Sept 2021. doi: 10.1021/acsomega.1c02670. [Online]. Available: <https://doi.org/10.1021/acsomega.1c02670>
- [31] T. Sönmez, S. J. Thompson, S. W. Price, D. Pletcher, and A. E. Russell, "Voltammetric studies of the mechanism of the oxygen reduction in alkaline media at the spinels Co₃O₄ and NiCo₂O₄," *J. Electrochem. Soc.*, vol. 163, no. 10, p. H884, July 2016. doi: 10.1149/2.0111610jes. [Online]. Available: <http://dx.doi.org/10.1149/2.0111610jes>
- [32] M. Hosseini and P. Zardari, "Electrocatalytical study of carbon supported Pt, Ru and bimetallic Pt-Ru nanoparticles for oxygen reduction reaction in alkaline media," *Appl. Surf. Sci.*, vol. 345, pp. 223-231, Aug 2015. doi: 10.1016/j.apsusc.2015.03.146. [Online]. Available: <https://doi.org/10.1016/j.apsusc.2015.03.146>
- [33] T. Sönmez, "Electrochemical performance and kinetics of Mn, Ni, Fe, and Co-loaded covalent triazine frameworks for oxygen evolution reaction in alkaline media," *Fuel*, vol. 403, p. 136106, 2026. doi: 10.1016/j.fuel.2025.136106. [Online]. Available: <https://doi.org/10.1016/j.fuel.2025.136106>
- [34] H. H. Hamzah, N. H. Saleh, B. A. Patel, M. M. Mahat, S. A. Shafiee, and T. Sönmez, "Recycling chocolate aluminum wrapping foil as to create electrochemical metal strip electrodes," *Molecules*, vol. 26, no. 1, p. 21, Dec 2020. doi: 10.3390/molecules26010021. [Online]. Available: <https://doi.org/10.3390/molecules26010021>
- [35] S. Xue, B. Garlyyev, A. Auer, J. Kunze-Liebhäuser, and A. S. Bandarenka, "How the nature of the alkali metal cations influences the double-layer capacitance of Cu, Au, and Pt single-crystal electrodes," *J. Phys. Chem. C*, vol. 124, no. 23, pp. 12442-

12447, June 2020. doi:
10.1021/acs.jpcc.0c01715. [Online].
Available:
<https://doi.org/10.1021/acs.jpcc.0c01715>

- [36] C. M. Schott, et al., "How to assess and predict electrical double layer properties. Implications for electrocatalysis," *Chem. Rev.*, vol. 124, no. 22, pp. 12391-12462, Nov 2024. doi:
10.1021/acs.chemrev.3c00806. [Online].
Available:
<https://doi.org/10.1021/acs.chemrev.3c00806>